

Supporting Information for

Probing the Deposition Kinetics of Nanoparticles by Plasmonic Imaging and Counting Single Nanoparticles

Hai-Bo Chen, Di Jiang, Yi-Nan Liu, Chen Qian, Xiao-Li Zhou, and Xian-Wei Liu*

CAS Key Laboratory of Urban Pollutant Conversion, Department of Applied
Chemistry, University of Science & Technology of China, Hefei 230026, China

*Corresponding author

E-mail: xianweiliu@ustc.edu.cn (XW Liu)

Supplementary Notes

Note S1: Effect of pH on nanoparticle deposition

Supplementary Figures

Figure S1: PS Nanoparticle characterization

Figure S2: Cumulative number of collision and deposition events of nanoparticles as a function of time

Figure S3: Collision rate, deposition rate and zeta potential as functions of electrolyte concentration

Figure S4: Collision rate, deposition rate and zeta potential as functions of solution pH

Figure S5: Attachment efficiency as a function of solution pH

Figure S6: Contact angle and pK_a of gold film surface decorated with different functional groups

Supplementary Tables

Table S1: Collision and deposition rates of nanoparticles on different functionalized surfaces

Supplementary Note

Note S1: Effect of pH on nanoparticle deposition

The collision and deposition kinetics of PS nanoparticles were examined in phosphate buffer (PB) solutions with pH ranging from 3-9. Low attachment rate of nanoparticles were observed when the solution pH was lower than 5, while there was a substantial increase in the deposited number of nanoparticles as the solution pH was higher than 5 at low ionic strength solution. (Figure S4A). To shed light on the mechanism of pH-dependent deposition, zeta potentials of PS nanoparticles with carboxylic groups were measured. The zeta potential was -30 mV at pH 9 and increased to -7 mV at pH 3 (Figure S4B). The isoelectric point of gold surface was 4.5.¹ Therefore, the negatively charged nanoparticles were repelled by the negatively charged surface when the pH was higher than 5. As the pH decreased, the charge on the gold surface was neutralized, resulting in the decrease of repulsion force. In contrast, the attachment efficiencies exhibited insensitive to solution pH variations in high ionic strength solution (Figure S5), indicating that the role of ionic strength is dominant in nanoparticle deposition.

Supplementary Figures

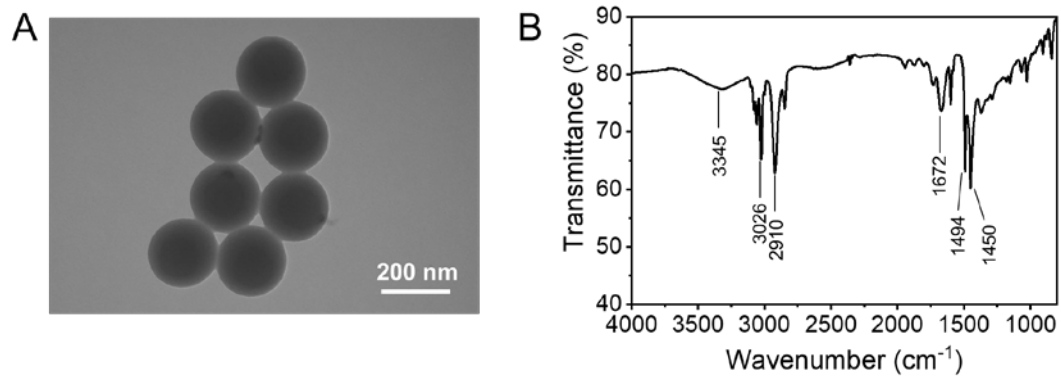


Figure S1. PS Nanoparticle Characterization. (A) TEM characterization and (B) IR spectrum of 200 nm carboxylate PS nanoparticles.

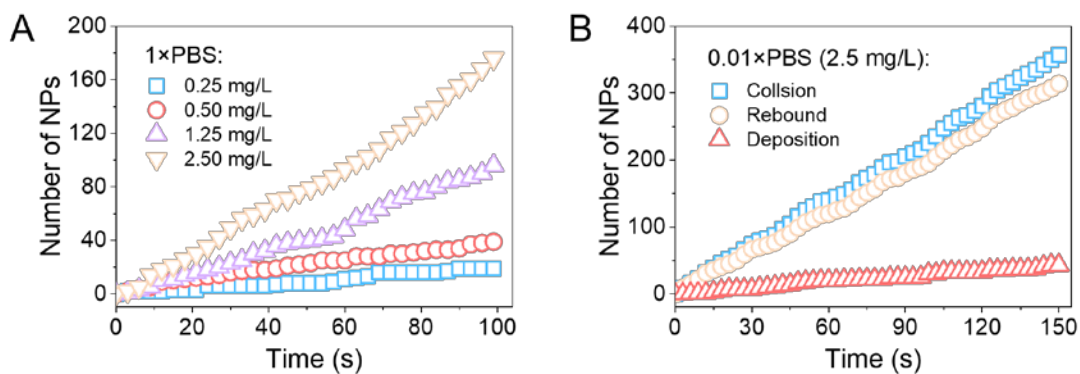


Figure S2. Cumulative number of collision and deposition events of nanoparticles

as a function of time. (A) Collision/deposition kinetic curves of nanoparticles with nanoparticle concentration ranging from 0.25 to 2.5 mg/L in 1xPBS solution. All the collision events led to a permanent adsorption/deposition on the surface. Thus, the cumulative nanoparticle number of collision and deposition were identical. (B) Collision, rebound and deposition nanoparticle number counts as a function of time in 0.01xPBS solution with nanoparticle concentration of 2.5 mg/L. Rebound events of nanoparticle existed due to electrostatic repulsion force, resulting cumulative deposition number of nanoparticles was lower than collision number of nanoparticles. In all cases, collision rate and deposition rate were calculated as the rate of change in the cumulative nanoparticle number of collision or deposition in a given time period.

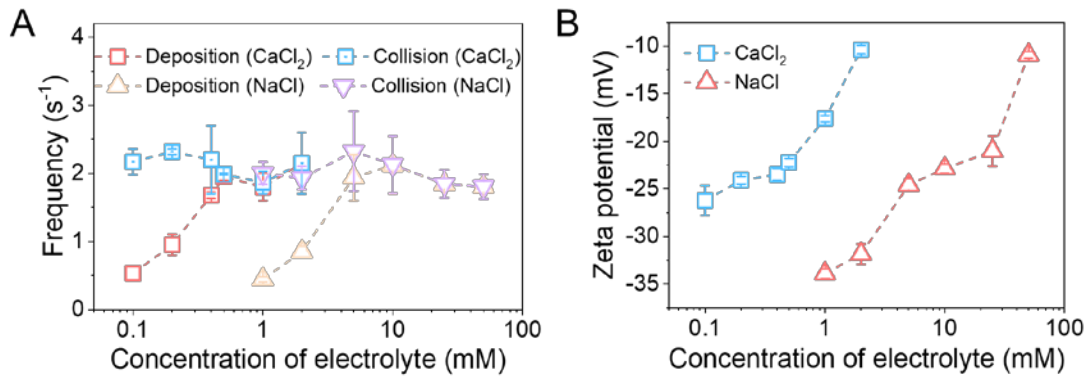


Figure S3. Collision rate, deposition rate and zeta potential as functions of electrolyte concentration. (A) Collision and deposition rates of nanoparticles as a function of NaCl and CaCl₂ concentration, respectively. An increase in the monovalent and divalent electrolyte concentrations led to a high deposition rate. Collision rate remained constant as ionic strength changed, indicating nanoparticle concentration was stable during the experiment. (B) Zeta potential as a function of NaCl and CaCl₂ concentration, respectively. An increase in the monovalent and divalent electrolyte concentrations led to the higher zeta potential. Test conditions: nanoparticle concentration = 2.5 mg/L, pH 7. Error bars represent standard deviations of duplicate measurements.

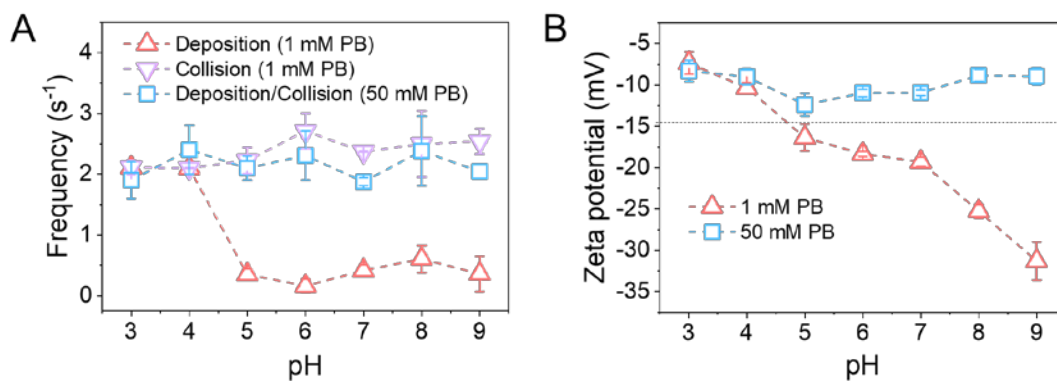


Figure S4. Collision rate, deposition rate and zeta potential as functions of solution pH. (A) Collision and deposition rates of nanoparticles as a function of pH in 1 mM PB and 50 mM PB, respectively. In 1 mM PB, for pH > 5, low attachment phenomenon of nanoparticles were observed. For pH < 5, there was a substantial increase in the deposited number of nanoparticles. In 50 mM PB, the collision and deposition rates were identical, indicating all collision events led to permanent adsorption/deposition on the surface. (B) Zeta potential as a function of pH in 1 mM PB and 50 mM PB, respectively. Noticeable changes of the zeta potential value were observed with pH adjustment in 1 mM PB. Zeta potential was stable with the change of pH in 50 mM PB. The dotted line represented the possible energy boundary. Test conditions: nanoparticle concentration = 2.5 mg/L. Error bars represent standard deviations of duplicate measurements.

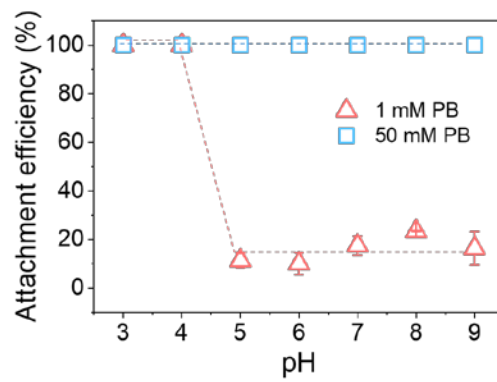


Figure S5. Attachment efficiency as a function of pH in 1 mM and 50 mM PB solutions.

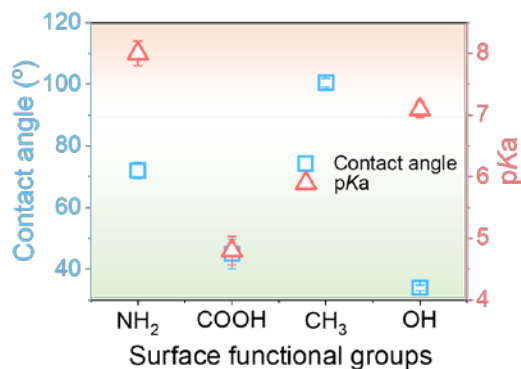


Figure S6. Contact angle and pKa of the surface coated with different functional groups. A 1 μL droplet was placed on the air-dried functionalized gold film surface, and contact angles were measured after 10 s. Three contact angle measurements on random locations in each sample were performed with deionized water at room temperature (20 $^{\circ}\text{C}$). The pK_a values of functional groups were obtained from the previous study.² The dotted line represents the boundary between hydrophilicity and hydrophobicity of the surface or the boundary between the positively charged and negatively charged surfaces under the test condition of pH 7. Error bars indicate one standard deviation.

Supplementary Tables

Table S1 Collision and deposition rates of nanoparticles on different functionalized surfaces

Functional groups	Ionic strength (mM)	Collision rate (s ⁻¹)	Deposition rate (s ⁻¹)
-NH ₂	1	2.20 ± 0.08	2.20 ± 0.08
	5	2.40 ± 0.40	2.40 ± 0.40
	10	1.82 ± 0.02	1.82 ± 0.02
-COOH	1	2.20 ± 0.20	0.01 ± 0.00
	5	2.06 ± 0.40	1.23 ± 0.43
	10	1.90 ± 0.10	1.58 ± 0.02
-CH ₃	1	1.93 ± 0.07	0.95 ± 0.05
	5	2.42 ± 0.02	2.42 ± 0.02
	10	1.98 ± 0.35	1.98 ± 0.35
-OH	1	1.79 ± 0.09	1.79 ± 0.09
	5	1.92 ± 0.24	1.92 ± 0.24
	10	1.73 ± 0.28	1.73 ± 0.28

References

- (1) Fears, K. P.; Creager, S. E.; Latour, R. A., Determination of the surface pK of carboxylic- and amine-terminated alkanethiols using surface plasmon resonance spectroscopy. *Langmuir* **2008**, *24*, 837-843.
- (2) Wang, Z.; Wang, X.; Zhang, J.; Yu, X.; Wu, Z., Influence of surface functional groups on deposition and release of TiO₂ nanoparticles. *Environ. Sci. Technol.* **2017**, *51*, 7467-7475.